Article:
Oliveira, AM, Lehman, JH orcid.org/0000-0001-6610-6519 and Lineberger, WC (2018) Photoelectron Spectroscopy of the Aminomethoxide Anion, $H_2C(NH_2)O^-$. Journal of Physical Chemistry A, 122 (22). pp. 4954-4962. ISSN 1089-5639

https://doi.org/10.1021/acs.jpca.8b02921

Photoelectron Spectroscopy of the Aminomethoxide Anion, $H_2C(NH_2)O^-$

Journal:	*The Journal of Physical Chemistry*
Manuscript ID	jp-2018-02921j.R2
Manuscript Type:	Special Issue Article
Date Submitted by the Author:	07-May-2018
Complete List of Authors:	Oliveira, Allan; University of Colorado, JILA and Chemistry and Biochemistry Lehman, Julia; University of Leeds, School of Chemistry Lineberger, W; University of Colorado, JILA and Chemistry

Photoelectron Spectroscopy of the Aminomethoxide Anion, $H_2C(NH_2)O^-$

Allan M. Oliveira,[†] Julia H. Lehman,[†,‡,*] and W. Carl Lineberger[†,*]

[†]*JILA and Department of Chemistry and Biochemistry, University of Colorado, Boulder, CO 80309, United States of America*

[‡]*School of Chemistry, University of Leeds, Leeds LS2 9JT, United Kingdom*

Abstract

We report the photoelectron spectrum of the aminomethoxide anion ($H_2C(NH_2)O^-$). The electron affinity (EA) of the aminomethoxy radical is determined to be 1.944(1) eV. Transitions to the ground ($\tilde{X}\ ^2A''$) and first excited ($\tilde{A}\ ^2A'$) electronic states of aminomethoxy are observed, with the term energy measured to be $T_0(\tilde{A} \leftarrow \tilde{X})$ = 0.085(1) eV. A long vibrational progression is observed for the transition to the ground $\tilde{X}\ ^2A''$ electronic state of aminomethoxy, primarily consisting of OCN bending and HNH wagging vibrations, leading to the assignment of these two fundamental vibrational frequencies of $H_2C(NH_2)O^{\bullet}$ $\tilde{X}\ ^2A''$. The gas phase acidity of aminomethanol is calculated at the G4 level of theory to be $\Delta_{acid}H^o_{0K}$ = 374.0 kcal mol^{-1}, which, when combined with the experimental EA of aminomethoxy in a thermochemical cycle, provides a determination of the O–H bond dissociation energy, $D_0(H_2C(NH_2)O–H)$ as 106(2) kcal mol^{-1}. Comparisons of the EAs and $T_0(\tilde{A} \leftarrow \tilde{X})$ for the aminomethoxy, methoxy, ethoxy, and hydroxymethoxy radicals provides insight into how the substituent group affects the electronic structure of singly substituted alkoxy radicals.

I. Introduction

Alkoxy radicals are an important class of molecules in atmospheric[1-5] and combustion[6-12] processes, where they often act as highly reactive intermediates. As an open-shell species with the radical center located on the oxygen, complicated further by some radicals possessing high symmetry, alkoxy radicals often have complex electronic structure making it difficult to fully characterize these molecules spectroscopically. Both their high reactivity and challenging electronic structure have motivated investigations of alkoxy radicals using a variety of experimental and theoretical methods.[13-19] Experimentally, alkoxy radicals have been studied in the gas phase mainly via spectroscopic techniques.[16, 20-27] Theoretically, the electronic structure of small alkoxy radicals have been investigated with a focus on Jahn-Teller interactions, spin-orbit splittings, and vibronic couplings.[28-31]

Several experimental investigations, including extensive work by Miller and coworkers,[32-35] have focused on building from the simplest alkoxy radical (methoxy) to larger alkyl substituted radicals, studying how the vibrational and electronic structure are altered upon the addition of different functional groups.[16, 32, 34-36] Ramond *et al.*[16] investigated the ethoxy ($H_2C(CH_3)O^{\bullet}$), isopropoxy ($HC(CH_3)_2O^{\bullet}$), and *tert*-butoxy ($C(CH_3)_3O^{\bullet}$) radicals via photoelectron spectroscopy of the corresponding anions, measuring their electron affinities (EA) and term energies ($T_0(\tilde{A} \leftarrow \tilde{X})$). For ethoxy, the term energy was measured as 355(10) cm^{-1} by Ramond *et al.*[16] via anion photoelectron spectroscopy, agreeing well with the more accurate term energy of 364(1) cm^{-1} subsequently measured by Jin *et al.*[33] via dispersed fluorescence spectroscopy. Upon further methyl substitution, forming isopropoxy, the term energy decreases to 68(10) cm^{-1}.[33] In addition to these examples, the hydroxymethoxy radical ($H_2C(OH)O^{\bullet}$) was investigated via anion photoelectron spectroscopy to study the effect of non-alkyl substitution.[37]

The hydroxymethoxy term energy was found to be $T_0(\tilde{A} \leftarrow \tilde{X}) \sim 3300$ cm^{-1}, close to an order of magnitude larger than ethoxy.[37] In the present work, we extend this series of studies by investigating the aminomethoxy radical ($H_2C(NH_2)O^{\bullet}$) via anion photoelectron spectroscopy of aminomethoxide ($H_2C(NH_2)O^-$) using electron velocity map imaging (VMI) and associated quantum chemical calculations. A comparison of the EA and $T_0(\tilde{A} \leftarrow \tilde{X})$ determinations provides instructive insight into the effect of substituent groups on the electronic structure of substituted alkoxy radicals ($H_2C(R)O^{\bullet}$, R = H, CH_3, NH_2 or OH).

However, the motivation to study the aminomethoxy radical and its corresponding anion extends beyond a fundamental chemical and electronic structure investigation. The aminomethoxide anion is the conjugate base of aminomethanol ($H_2C(NH_2)(OH)$), an important prebiotic molecule as a precursor to simple amino acids.[38-39] Spectroscopic studies of aminomethanol are non-existent, due to its inherent instability in the gas phase.[40-41] By approaching the spectroscopy of aminomethoxy via its anion, the EA of aminomethoxy is able to be measured. The O–H bond dissociation energy in aminomethanol can then be obtained in a thermochemical cycle using the measured EA of aminomethoxy in conjunction with the gas phase acidity of aminomethanol.[42]

II. Methods

a) Experimental

In this experiment, an electron velocity-map imaging (VMI) spectrometer is used, which is described in detail elsewhere.[43] Briefly, the apparatus consists of four major components: anion generation, mass separation, mass-selected anion photodetachment, and measurement of

the kinetic energy and angular distributions of the photodetached electrons using the VMI spectrometer.

The aminomethoxide anion ($H_2C(NH_2)O^-$, m/z=46) is produced via the association reaction involving the amide anion (NH_2^-) and formaldehyde (H_2CO). The ions are produced using a dual pulsed valve plasma entrainment source, which has been described in detail elsewhere.[44] This source consists of two orthogonally oriented pulsed General Valves (Parker-Hannifin Series 9): a main supersonic expansion of ~1% H_2CO in argon gas (40 psig), and a secondary expansion (35 psig) of a mixture of 10% NH_3 (99.999% purity) in argon. This secondary expansion only accounts for approximately 10% of the total pressure rise in the vacuum chamber when both valves are operational. The secondary expansion features a pulsed parallel plate discharge (ΔV = -2 kV, Δt ~130 μs), generating a plasma which is then entrained into the main expansion. The primary anion formed in this discharge is NH_2^-, which is able to react with neutral H_2CO upon plasma entrainment into the main expansion. The excess argon in the main supersonic expansion provides collisional quenching, stabilization, and cooling of the product anions. The major products from this process, specifically anions with m/z = 46, will be described in Section III.a.

Downstream from the main expansion, the anions are extracted into a Wiley-McLaren time-of-flight (WM-TOF) mass spectrometer where they are steered, focused, and separated by their mass-to-charge ratio (m/z). At the focus of the WM-TOF spectrometer, the anions are spatially intersected with a laser pulse, which is appropriately timed to temporally overlap with anions of a particular m/z ratio. This generates a small volume of photodetached electrons which are perpendicularly extracted into a VMI photoelectron spectrometer. The 3D electron distribution is velocity focused onto a 2D position sensitive microchannel plate (MCP)/phosphor

screen detector. The resulting 2D image is transformed into a 1D photoelectron speed distribution using the MEVELER program.[45] The electron speed distribution is then converted to electron kinetic energy (eKE) distribution through a Jacobian transformation. Since the eKE distribution depends on the photon energy used for detachment, we report photoelectron spectra as a function of decreasing electron binding energy (eBE = hν – eKE), which is independent of photon energy.

The angular distribution of the photoelectrons with respect to the laser polarization vector is also extracted from the velocity-mapped image. By fitting the observed angular distribution to the functional form given by Cooper and Zare,[46] the anisotropy parameter (β) is obtained. The β parameter provides information on the nature of the orbital from which the electron originated, and is a powerful tool for identifying different electronic states of molecules or atoms. This anisotropy parameter is calculated within the MEVELER program. More information can be found in a recent review[47] of photoelectron angular distributions and applications to the analysis of photoelectron spectra.

In a VMI spectrometer, the resolution improves as the eKE decreases.[48] In order to take advantage of this characteristic property, we employ several different photon energies. Specifically, we use the second and third harmonics of a pulsed Nd:YAG laser: hν = 2.329 eV (532.3 nm) and 3.494 eV (354.8 nm), respectively. In addition, photon energies of 2.172 eV (570.8 nm) and 2.038 eV (608.4 nm) are also employed, and are generated by a 354.8 nm pumped optical parametric oscillator. The limits of our instrument resolution are determined by the photoelectron spectrum of an atomic anion, which is S^- for this experiment,[49] using the above photon energies. When considering eKE $\gtrsim$ 0.4 eV, the ratio between peak full width at half maximum (*fwhm*) and eKE reaches a constant value of ~3%. For eKE approaching 0 eV, the

instrument reaches a constant resolution (peak *fwhm*) of approximately 3 meV. In general, the width of an individual peak is approximately described by *fwhm* ~ (0.003 + 0.03 × eKE) eV. An experimental peak with a *fwhm* that is approximately within these parameters, which are determined for each experiment based on the S^- photoelectron spectrum, is referred to as being "resolution-limited."

Throughout this work, the uncertainties in the reported peak positions are derived from the uncertainties associated with the measurement of the photon energy, the statistical error in fitting the peaks to Gaussian functions, the absolute energy scale calibration, which uses the known photoelectron spectrum of S^-,[49] and the number of independent measurements of the individual peaks. These uncertainties are considered to be independent of one another and therefore are added in quadrature and result in uncertainties of approximately 1 meV. However, the reported error associated with the measurement of a specific spectroscopic transition can exceed this statistical estimate for several reasons. First, since our experimental resolution does not allow for detection of individual transitions, the center of an observed peak does not necessarily correspond to the band origin of a transition. In order to account approximately for this shift, the procedure developed by Engelking[50-51] for rotational band shifts is employed (see Supporting Information). This small shift is included in the reported measurements of vibrational frequencies, the EA, and $T_0(\tilde{A} \leftarrow \tilde{X})$. Second, many of the observed peaks are not resolution limited and are therefore subject to further broadening. Specifically, more than one vibrational transition can account for the width of the peaks, and hence when assigning a transition to a non-resolution limited peak, the actual band origin of that transition may reasonably be located within the *fwhm* of that peak. Therefore, for these cases, we use the peak half-width-at-half-maximum (± *fwhm*/2) to provide a conservative uncertainty in the energy of a vibrational component of

such a transition. Where appropriate, this additional uncertainty is included in the reported error bars. For the reported β values in Figures, the β values shown correspond to average values across the top ¼ of each peak in order to minimize the contribution from neighboring peaks to the β of individual peaks. The error bars correspond to the standard deviation of the mean β values across the points averaged for each peak.

b) Theoretical

Quantum chemical calculations that did not require the use of high level methods were performed in the Gaussian 09 suite of programs.[52] The enthalpies for the reaction ($\Delta_{rxn}H^{o}_{0K}$) between NH_2^- and H_2CO forming various structural isomers of H_4CNO^- (m/z=46) together with the EAs of the neutral products (see Supporting Information) were calculated using B3LYP/aug-cc-pVTZ. The energy of excited electronic states of the aminomethoxide anion were calculated using EOM-CCSD/aug-cc-pVTZ.

The electronic structure calculations used for the generation of simulated photoelectron spectra were carried out with energies and geometries determined using the Molpro suite of programs.[53] Specifically, geometry optimization and harmonic vibrational normal mode calculations for the ground electronic states of aminomethoxide and aminomethoxy were performed using the CCSD(T)/aug-cc-pVTZ (ROCCSD(T) for the neutral radical) level of theory. The multiconfigurational self-consistent-field (MCSCF) method with the aug-cc-pVTZ basis set was used for the excited electronic state of aminomethoxy ($\tilde{A}\,^2A'$). In this calculation, the complete active space method (CASSCF) was used for geometry optimization and calculation of the harmonic vibrational normal modes. The optimization results are provided in the Supporting Information (Tables S1 – S4). For the MCSCF calculations, an active space consisting of five electrons in four orbitals (CAS(5,4)) was employed. The orbitals in the active

space nominally correspond to the σ(CO), oxygen $2p_y$ and $2p_x$, and σ*(CO) orbitals. A range of active spaces were considered, from very small (3,2) to very large (19,10), including a (7,5) active space which encompassed the lone electron pair on nitrogen. All of the active spaces gave similar excitation energies (the EA of $H_2C(NH_2)O^{\bullet}$ and its $T_0(\tilde{A} \leftarrow \tilde{X})$ term energy), but we report using the (5,4) active space as successfully employed by Dillon and Yarkony for other small methoxy radicals. The (5,4) active space has the same number of electrons, and number and type of orbitals as was used by Dillon and Yarkony for ethoxy[54] and hydroxymethoxy.[55] Given the high degree of success with this previous work on similar systems and the smaller computational cost, the (5,4) active space was chosen. This method for the excited state was chosen instead of a coupled-cluster approach as in the neutral ground state due to the successful calculations reported in previous work by Dillon and Yarkony when calculating excited states of substituted alkoxy radicals.[54-56] They achieved success in reproducing the experimental data where non-multireference methods failed,[16, 54] meaning that the multireference method provides a more accurate representation of the electronic structure involved. This computational method is also nicely balanced between accuracy and computational expense. However, we found that using the higher level CCSD(T)/aug-cc-pVTZ calculations for the $H_2C(NH_2)O^-$ $\tilde{X}$ and $H_2C(NH_2)O^{\bullet}$ $\tilde{X}$ states, in combination with the CASSCF approach for the $H_2C(NH_2)O^{\bullet}$ $\tilde{A}$ state, showed a significantly better agreement with experiment compared to a fully CASSCF approach for the $H_2C(NH_2)O^-$ $\tilde{X}$ and $H_2C(NH_2)O^{\bullet}$ $\tilde{X}$, $\tilde{A}$ states. Finally, we calculated the $H_2C(NH_2)O^{\bullet}$ term energy, $T_0(\tilde{A} \leftarrow \tilde{X})$, using the state averaged multireference configuration interaction with explicitly correlated energies (SA MRCI-F12), where the geometries and zero-point energies (ZPE) are obtained from the CAS optimization for the neutral $\tilde{X}$ and $\tilde{A}$ states.

The photoelectron spectra are calculated using the ezSpectrum[57] program. The spectra were simulated using the equilibrium geometries, harmonic frequencies, and normal mode vectors of aminomethoxide and aminomethoxy obtained from the *ab initio* calculations described above in order to calculate the appropriate Franck–Condon (FC) factors. In the simulation, the FC factors are calculated within the harmonic oscillator approximation and by employing the Sharp-Rosenstock-Chen method with Duschinsky rotations.[58] These calculations were carried out assuming an anion temperature of 150 K, based on previous experiments.[37, 59] This procedure generates a discrete spectrum of sticks, where the intensities correspond to the calculated FC factor and the positions correspond to transitions between the relevant anion and neutral vibrational levels. In order to make a direct comparison between the calculation and experiment, the stick spectrum is convolved with Gaussian functions where the integrated area is equal to the calculated transition intensity and the *fwhm* is consistent with the eKE-dependent instrumental resolution of the VMI spectrometer.

III. Results

a) Chemical characterization of the observed anion with m/z=46

Following the procedure described in Section II.a, the mass spectrum confirmed the production of an anion with m/z=46. The identity of m/z=46 was verified by the following series of tests. The anion with m/z = 46 was only observed when both H_2CO was in the main expansion gas mixture and NH_3 was in the side (discharge) expansion gas mixture. If only argon is present in the main expansion, the discharge of NH_3 in the side expansion gas mixture generates a large amount of NH_2^- anions. NH_2^- is a strong base capable of deprotonating H_2CO[60] whereas other anions generated in the NH_3 discharge are not thermodynamically capable of doing so. When H_2CO is added to the main expansion gas mixture, the reaction of NH_2^- with H_2CO is expected

to cause a deprotonation of formaldehyde.[61] Indeed, m/z=29 was observed and found to be HCO^-. In addition to deprotonating formaldehyde, NH_2^- can also react with formaldehyde in an association reaction, forming m/z=46. This reaction product can be collisionally cooled and stabilized by the argon carrier gas present in abundance in the main expansion.

In the association reaction between NH_2^- and H_2CO, the formation of a C–N bond is the most likely to occur, resulting in the aminomethoxide anion being formed (inset graphic of Fig. 1). While the physical intuition that the association reaction is most likely to produce m/z=46 as the aminomethoxide anion, a comparison between the experimental results and the theoretical predictions of the EAs of various other possible isomers further confirms this (see Supporting Information). The calculations performed here (CCSD(T)/aug-cc-pVTZ) predict the EA of aminomethoxy as 1.89 eV, in good agreement with the observed EA of 1.944 eV (see Section III). Other structural isomers of H_4CNO that could possibly arise from photodetachment from other association reaction products between NH_2^- and H_2CO possess EAs at least 0.6 eV lower than what is predicted for aminomethoxy (see Supporting Information). However, no photoelectron signal was observed below an electron binding energy of approximately 1.9 eV, suggesting that it is highly unlikely that these other isomers are being formed in any significant abundance. While this observation allows for a very strong inference that the identity of m/z=46 is aminomethoxide, this will be further substantiated by the agreement between experimental observation and theoretical predictions of its photoelectron spectrum.

b) Overview and electron affinity of aminomethoxy

Given that the EA of NH_2 (0.771 eV)[62] is substantially less than that of O (1.461 eV),[63] the negative charge on aminomethoxide is likely to be largely localized on the oxygen atom, as with the other alkoxide anions.[16, 37, 48, 64] Thus, the EA of the aminomethoxy radical should be

similar to the other alkoxy radicals,[16, 37, 48, 64] *i.e.* near 2 eV. In addition, this formal negative charge on the oxygen causes a strong intramolecular electrostatic interaction between the oxygen and the amino group. Upon electron photodetachment, it is expected that the strength of the intramolecular interaction will be significantly lessened, causing geometry changes associated with the weakening of this interaction. For example, the OCN angle and the distance between the oxygen atom and the amino group hydrogen atoms would be larger for the neutral radical compared to the anion. The calculated equilibrium geometries of aminomethoxide and aminomethoxy are detailed in Table S1 and support this physical interpretation. These changes in structural parameters will lead to vibrational transitions involving excitation of the HNH wag, OCN bend, and OC or CN stretches. If there is a sufficiently large degree of structural change, this could result in a photoelectron spectrum showing an extended vibrational progression. It is also likely that transitions involving a low-lying excited electronic state would be observed, as is the case with other substituted alkoxide photoelectron spectra. Given that the $T_0(\tilde{X} \leftarrow \tilde{A})$ for other alkoxy radicals range from approximately 70 cm^{-1} to 3300 cm^{-1}, it might be expected that the $T_0(\tilde{X} \leftarrow \tilde{A})$ for aminomethoxy would lie somewhere within this range. In the following sections, results from the experiment are presented, the EA and $T_0(\tilde{X} \leftarrow \tilde{A})$ of aminomethoxy are determined, along with several vibrational frequencies.

The lower panel of Fig. 1 displays the photoelectron spectrum of aminomethoxide acquired with a photon energy of 3.494 eV, which covers the complete range of eBE wherein photoelectron signal was observed. The wavelengths utilized for acquiring the spectra are numbered according to the figure where the resulting spectra are shown, *i.e.* $h\nu_1$ corresponds to the photon energy employed to acquire the spectrum shown in Fig. 1. Fig. 1 displays a spectrum which begins with a sharp peak A, at an eBE of ~1.94 eV, with a resolution limited width of 48

meV, followed by partially resolved peaks B – D, which will be discussed below. The rest of the spectrum has partially resolved structure with peaks extending to an eBE of approximately 3.0 eV, where the resolution should have improved to ~ 15 meV. The fact that there are no clearly resolved peaks at the highest eBE (lowest eKE) part of the spectrum indicates that there is likely a large degree of spectral congestion in this photoelectron spectrum.

The upper panel of Fig. 1 shows the anisotropy parameter (β) of the photoelectron spectrum (black circles). The anisotropy parameter is generally positive for the entire progression, becoming more positive with higher eBE. However, there are also several negative values of β, which correspond to the peaks labeled A and C. When this observation is compared to the overall positive β of the rest of the progression, it strongly suggests that two distinct electronic states of aminomethoxy are accessed following the 3.494 eV electron photodetachment of aminomethoxide. In order to analyze this spectrum further, photoelectron spectra with higher resolution are required, and hence we obtain a second spectrum using a lower photon energy.

The photoelectron spectrum acquired with a photon energy of 2.172 eV (570.8 nm) is presented in Fig. 2. This higher resolution spectrum should capture peaks A – D on the rising edge of the low eBE portion of the spectrum shown in Fig. 1. Indeed, there are now a number of better resolved peaks between 1.94 and 2.17 eV eBE, in contrast to the spectrum shown in Fig. 1. Notice that what were barely resolvable peaks labeled B – D in Fig. 1 are now seen to consist of groups of peaks indicated in Fig. 2 under brackets with the same labels, supporting the conjecture that the lack of resolvable peaks when employing the 3.494 eV photon energy (Fig. 1) was due to spectral congestion. The 11 resolved peaks are now labeled with lowercase letters and numbers corresponding to the unresolved bands of Fig. 1. In this new spectrum, the *fwhm* of

peak a1 is 13 meV, significantly narrower than peak A in Fig. 1 (48 meV), but continues to be close to resolution limited. This again indicates that peak a1 (peak A in Fig. 1) is likely dominated by a single vibrational transition, a statement that is confirmed by the simulated photoelectron spectrum displayed in the lower panel of Fig. 2.

For the determination of the EA of aminomethoxy, we focus on peak a1 of Fig. 2, which is the apparent origin of the overall vibrational progression. As mentioned previously, the CCSD(T)/aug-cc-pVTZ calculations predict the EA of aminomethoxy as 1.89 eV, in close agreement with the corresponding eBE of the center of peak a1. In order to establish our best measurement of the EA of aminomethoxy, we obtain a photoelectron spectrum with an even lower photon energy of 2.038 eV, displayed in Fig. 3. Using this lower photon energy, peak a1 has a *fwhm* of 9 meV. From the center position of peak a1 and the consideration of the uncertainties and shift discussed in Section II, the EA of aminomethoxy is determined to be 1.944(1) eV. Other important assignments are based on Figs. 2 and 3 and partially rely on a comparison between the experimental and simulated photoelectron spectra.

The simulation shown in the lower panel of Fig. 2 assists in determining the transition assignments of the other observed peaks in the experimental photoelectron spectrum. In the simulation, the red sticks represent transitions from the ground electronic state of aminomethoxide to the ground electronic state of neutral aminomethoxy ($\tilde{X}$) and the blue sticks represent transitions to the neutral excited electronic state ($\tilde{A}$), which is discussed in the following section (III.c). The "stick spectra" representing transitions to these two states were shifted and scaled so that the origin transitions of the $\tilde{X}$ and $\tilde{A}$ states of aminomethoxy matched the position and ratio of the areas of peaks a1 and b2, respectively. The qualitative agreement between experiment and calculation supports the claim that the ground state origin transition

(peak a1) is dominated by a single vibrational transition and hence allowed for a precise measurement of the EA. From a comparison between the higher resolution spectra (Figs. 2 and 3) and simulation, a thorough analysis of the spectrum can be performed, providing the measurement of $T_0(\tilde{X} \leftarrow \tilde{A})$ and assignments of vibrational frequencies of aminomethoxy.

c) Determination of the term energy, $T_0(\tilde{A} \leftarrow \tilde{X})$, of aminomethoxy

The experimental assignment of the origin of the $\tilde{A}$ state vibrational progression is determined from three factors: experimental peak-specific anisotropy parameters, experimental peaks unable to be assigned to $\tilde{X}$ state transitions, and comparison with the theoretically predicted photoelectron spectra. In the spectrum obtained with a photon energy of 3.494 eV (Fig. 1), the $\tilde{X}$ state origin peak (peak A) has a $\beta < 0$, while the high eBE region (above ~2.2 eV) has β values that are greater than 0. As previously mentioned, this changing anisotropy parameter across the spectrum suggests the presence of transitions to at least two different electronic states. The high eBE region is likely dominated by transitions to the higher-lying $\tilde{A}$ state, which is confirmed by the calculated spectrum over the full range of eBEs (shown in Fig. S3 in the Supporting Information). However, because of the reduced resolution, the origin of the $\tilde{A}$ state vibrational progression cannot be determined from the spectrum in Fig. 1. From the higher resolution photoelectron spectrum (Fig. 2), an analysis of the β parameter shows that most of the observed peaks have a near isotropic photoelectron angular distribution ($\beta \approx 0$), apart from peak b2 with $\beta \approx +0.5$. A photoelectron spectrum obtained with a slightly higher photon energy of 2.329 eV (Fig. S2) further corroborates this observation of the positive anisotropy of peak b2 compared to neighboring peaks.

Peak b2 is the lowest eBE peak that does not have an assignment corresponding to a transition from the anion to the ground $\tilde{X}$ state of the neutral radical, according to the simulated photoelectron spectrum. Peak b2 is centered at 2.0294(7) eV (Fig. 3), 689(10) cm^{-1} above the $\tilde{X}$ state origin. While this peak spacing is similar to the HCH torsional frequency of the $\tilde{X}$ state (666 cm^{-1}, see Table S3), transitions involving this symmetry breaking vibrational mode are not allowed except through the possibility of significant vibronic coupling between the $\tilde{X}$ and $\tilde{A}$ states of aminomethoxy. There are no other predicted transitions to the ground $\tilde{X}$ state with significant Franck-Condon factors that could be assigned to peak b2. Additional resolved peaks in both Fig 2 and Fig S2 are similarly unassigned when only considering predicted transitions to the ground $\tilde{X}$ state with significant Franck-Condon factors, such as peaks d1 and d2. However, if peak b2 is assumed to be the $\tilde{A}$ state origin transition, and the theoretically predicted photoelectron simulation is overlaid with the experimental data, the simulation is able to capture these previously unassigned resolved peaks. This assignment is further confirmed by the overall satisfactory agreement between the calculated and experimental spectra over the full range of eBEs (Fig. S3). This agreement is particularly good with regard to the overall width of the vibrational envelope and the position of its maximum, located at approximately 2.28 eV eBE.

It is the confluence of these observations which allows us to assign peak b2 as the $\tilde{A}$ state origin transition. Thus, the $T_0(\tilde{A} \leftarrow \tilde{X})$ term energy is obtained from the highest resolution spectrum (Fig. 3) and is determined to be 0.085(1) eV. The calculations performed here (CAS(5,4)//MRCI-F12/aug-cc-pVTZ) find that the $T_0(\tilde{A} \leftarrow \tilde{X})$ term energy of aminomethoxy is 0.201 eV. Although the agreement with the experimental measurement is not completely satisfactory, possibly due to the small energy difference between the $\tilde{A}$ and $\tilde{X}$ states (see section

IV.b) and the use of a less computationally expensive active space, the experimental evidence of the origin of the ground and first excited electronic states is clear.

d) Vibrational analysis

In order to conduct a vibrational analysis of the experimental photoelectron spectrum, we compare the experimental and calculated spectra displayed in the lower panels of Fig. 2. For convenience, the transition energies are given relative to the specified electronic state's vibrational origin ($\tilde{X}$ or $\tilde{A}$) and reported in wavenumbers, therefore representing the vibrational frequencies of the final neutral electronic state. As mentioned in the beginning of Section III.b, the calculations predict that the most active vibrations in the photoelectron spectrum will be the HNH wag, OCN bend, C–N and O–C stretches based on the geometry change between the anion and neutral $\tilde{X}$ and $\tilde{A}$ states. As the subsequent analysis shows, our experimental observations indeed confirm our predictions, providing further confidence in the assignments made here.

Peak b1 is separated from peak a1 by 496(10) cm^{-1}, a value that agrees well with the calculated OCN bend harmonic frequency (498 cm^{-1}) of the neutral $\tilde{X}$ state. This provides a measurement of the OCN bending frequency $\nu_{14}(\tilde{X})$ = 496 (10) cm^{-1}. The transition which is predicted to dominate peak b3 can be assigned as $\nu_{12}(\tilde{X})$ = 790(20) cm^{-1}, which agrees well with the calculated harmonic frequency of the HNH wag (847 cm^{-1}). The assignments of peaks c1 through d3 are more complicated due to the presence of several transitions whose proximity would make them impossible to experimentally separate due to the instrument resolution. This spectral congestion limits our ability to assign some peaks to a single transition, and so tentative assignments are made instead (Table S7). As an example, peak c1 is located 985(12) cm^{-1} from the $\tilde{X}$ state origin, which can correspond to either the first overtone of the OCN bend in the

ground electronic state, $2\nu_{14}(\tilde{X})$, calculated as 996 cm^{-1}, or the C–O stretch $\nu_{11}(\tilde{X})$, calculated as 1002 cm^{-1}. These two transitions are predicted to have very similar Franck-Condon factors, further complicating the assignment. The ambiguity cannot be eliminated with our experimental resolution which limits our capability of accurately determining the source of these transitions.

e) Unassigned transitions

The high resolution photoelectron spectrum in Fig. 3 reveals two additional peaks, labeled * and **, which are not accounted for in the calculated spectrum. The spacings from peak a1 to peaks * and ** are 220(30) cm^{-1} and 350(40) cm^{-1}, respectively. The lowest frequency vibration of the $\tilde{X}$ state of aminomethoxy is the HNH torsion, calculated to be 252 cm^{-1}. While this vibrational frequency matches the peak spacing fairly well, this is a symmetry-forbidden transition. This suggests that the appearance of these peaks could be an indication of vibronic coupling between the $\tilde{X}$ and $\tilde{A}$ states of aminomethoxy. However, these peaks are not able to be resolved when using a higher photon energy (such as in the spectra reported in Figs. 2 and S2), but otherwise using the same experimental conditions. The photon energy-dependent appearance of these peaks suggests that peaks * and ** likely result from electron autodetachment, as described in previous investigations.[65-73] It is possible that the normally forbidden torsional mode gains intensity via the autodetachment process.[67, 73]

IV. Discussion

a) Thermochemistry of aminomethanol

Some thermochemical properties of aminomethanol can be obtained using the measured EA of aminomethoxy and a thermochemical cycle:[42]

$$D_0\left(H_2C(NH_2)O\text{–}H\right) = \Delta_{acid}H^{o}_{0K}(H_2C(NH_2)OH) - IE(H) + EA(H_2C(NH_2)O^{\bullet}) \quad (1)$$

There is no experimental measurement of either the O–H bond dissociation energy, $D_0(H_2C(NH_2)O–H)$, or the gas phase acidity, $\Delta_{acid}H^o_{0K}(H_2C(NH_2)OH)$, of aminomethanol. Thus, quantum chemical calculations must be employed to obtain either one of these values. In this work, $\Delta_{acid}H^o_{0K}(H_2C(NH_2)OH)$ was selected since this quantity only depends on calculating the heats of formation of the closed shell species $H_2C(NH_2)O^-$, $H_2C(NH_2)OH$, and H^+. The G4 composite method was applied yielding $\Delta_{acid}H^o_{0K}(H_2C(NH_2)(OH)) = 374.0$ kcal mol^{-1}, where the estimated uncertainty is on the order of 2 kcal mol^{-1}.[74] Using the experimental EA($H_2C(NH_2)O^{\bullet}$) = 1.944(1) eV and the well-known ionization energy of atomic hydrogen,[75] this cycle predicts $D_0(H_2C(NH_2)O–H)$ to be 106.3 ± 2.0 kcal mol^{-1}, using a conservative estimate of the uncertainty. This value for the bond strength, derived from a combination of experimental EA and the $\Delta_{acid}H^o_{0K}$ calculation is also in good agreement with the calculated (G4 composite method) value of $D_0(H_2C(NH_2)O–H) = 107.7$ kcal mol^{-1}. Thus, the thermochemical cycle is self-consistent when the experimental EA is combined with either of the calculated bond strength or acidity. Table 1 summarizes this result, together with other major experimental results reported here.

b) Comparison of aminomethoxy with other singly substituted alkoxy radicals

It is instructive to compare of the EAs of ethoxy, aminomethoxy, and hydroxymethoxy, as well as the unsubstituted methoxy. While these are isoelectronic radicals and have similar atom connectivity, each have different functional groups attached to the central carbon atom. Comparing the experimentally measured EAs of $H_2C(R)O^{\bullet}$ we see a trend of increasing EAs with increasing electronegativity of the R group: 1.5689(7),[64] 1.712(4),[16] 1.944(1), and 2.220(2)[37] eV for R=H, CH_3, NH_2, and OH, respectively. This trend can also be associated with the increasing strength of the intramolecular interaction between the R group and the adjacent oxygen. Although calculations show that both neutral and anions are stabilized by such an

interaction, the anions are stabilized more due to the greater coulombic character of the intramolecular bond. It is thus reasonable that the most electronegative group (R = OH) results in the largest EA. While the reason is unclear, the measured $T_0(\tilde{A} \leftarrow \tilde{X})$ values also correlate with the increasing electronegativity of the R group: 62(1) cm^{-1},[20] 364(1) cm^{-1},[33] 689(10) cm^{-1}, and approximately 3300 cm^{-1},[37] for R= H, CH_3, NH_2, and OH, respectively. For methoxy, the energy difference being referred to here is the spin-orbit splitting of ~ 60 cm^{-1},[64] a very distinct feature of the electronic structure in methoxy compared to what is observed for the substituted alkoxy radicals. Table 2 compares the measured EAs and $T_0(\tilde{A} \leftarrow \tilde{X})$ of small substituted alkoxy radicals, where the trend can be more easily noted.

It is also interesting to note that the photoelectron spectra of aminomethoxide and hydroxymethoxide[37] are quite similar, as shown in Fig. S4 in the Supporting Information. In fact, it appears as though the electronic excited state portion of the spectra were simply "shifted" to account for the difference in the term energies for the two molecules ($T_0(\tilde{A} \leftarrow \tilde{X})$ = 0.085(1) eV for aminomethoxy and $T_0(\tilde{A} \leftarrow \tilde{X})$ ~ 0.4 eV for hydroxymethoxy[37]). This five-fold difference between the $T_0(\tilde{A} \leftarrow \tilde{X})$ suggests that exchanging the amino group for a hydroxyl group has a significant effect on the electronic structure of these singly substituted alkoxy radicals. In addition to the their work on ethoxy,[54] Dillon and Yarkony performed a theoretical study of hydroxymethoxy[55] focusing on its distinct electronic structure. In that study, they argue that the electronic structure and the topography of the $\tilde{X}$ and $\tilde{A}$ states of hydroxymethoxy are drastically different from the typical Jahn-Teller influenced topography of ethoxy. This difference is mainly attributed to the strength of the intramolecular interaction between the hydroxyl group and the oxygen atom. In aminomethoxy, the amino group is also able to form a strong electrostatic intramolecular interaction with the O moiety, but the nitrogen atom is less electron-withdrawing

than oxygen and, therefore, polarizes the hydrogen atoms to a lesser extent. Aminomethoxy also exhibits an equilibrium geometry in which the hydrogen atoms are not as close to the O moiety when compared to hydroxymethoxy. This is because of the average geometry of hydroxymethoxy forms a four-membered planar O-C-O-H ring, while in aminomethoxy, the oxygen bisects the HNH angle, causing both hydrogens of the amino group to be out of the O-C-N plane. Thus, the interatomic distances between the hydrogen and the opposite oxygen atom are 2.68 Å in aminomethoxy versus 2.29 Å in hydroxymethoxy, which can make the interaction between these moieties considerably weaker in aminomethoxy than hydroxymethoxy.

A comparison between aminomethoxy and other small substituted alkoxy radicals provides a possible explanation of why the calculated and experimental photoelectron spectra presented in Fig. 2 have a less than perfect agreement, particularly for peaks above 2.06 eV. Is has been shown previously that for other small alkoxy radicals, the inclusion of vibronic coupling, *i.e.* coupling of electronic and vibrational degrees of freedom, was the primary contributor to generating accurate calculated photoelectron spectra.[37, 54-56] Similar to aminomethoxide, the photoelectron spectrum of ethoxide reported by Ramond *et al*.[16] displayed numerous prominent disagreements between harmonic calculations and the experiment, particularly regarding peak intensities. This photoelectron spectrum was later investigated by Dillon and Yarkony,[54] who, by including vibronic coupling between the ethoxy $\tilde{X}$ and $\tilde{A}$ states in the calculation, significantly increased the level of agreement between theory and experiment while also shedding light on why there were initially disagreements. Thus, it is likely that vibronic coupling between the $\tilde{X}$ and $\tilde{A}$ states in aminomethoxy is also a dominant contributor to the disagreement between calculation and experiment for the photoelectron spectrum of

aminomethoxide. However, it is beyond the scope of this work to attempt this level of theory for aminomethoxy.

V. Conclusions

In this work, the aminomethoxide ($H_2C(NH_2)O^-$) anion was successfully produced via an association reaction between the amide anion (NH_2^-) and formaldehyde (H_2CO). The photoelectron spectrum of $H_2C(NH_2)O^-$ obtained with a photon energy of 3.494 eV accesses the ground ($\tilde{X}\ ^2A''$) and first excited ($\tilde{A}\ ^2A'$) electronic states of the neutral aminomethoxy radical ($H_2C(NH_2)O^\bullet$). The photoelectron spectrum accessing these two electronic states of $H_2C(NH_2)O^\bullet$ is broad, extending for approximately 1 eV. The extent of the progression indicates that there is a large degree of geometry change between anion and neutral electronic states upon photodetachment. Higher resolution photoelectron spectra obtained using photon energies of 2.172 or 2.038 eV resolve vibrational transitions between the anion ground state and the neutral ground ($\tilde{X}\ ^2A''$) and excited ($\tilde{A}\ ^2A'$) electronic states. The high resolution photoelectron spectrum provides an experimental measurement of the electron affinity of aminomethoxy to be 1.944(1) eV) and the $T_0(\tilde{A} \leftarrow \tilde{X})$ term energy to be 0.085(1) eV. Several vibrational assignments were made, aided by a comparison between the experimental and calculated spectra. There is predicted to be strong Franck-Condon activity mainly in the OCN bending and HNH wagging vibrations of aminomethoxy. Some discrepancies between calculated and experimental peak intensity ratios were observed. Because of the small energy separation between the $\tilde{X}\ ^2A''$ and $\tilde{A}\ ^2A'$ states of aminomethoxy, and following a comparison with the ethoxy radical, it is suggested that not including vibronic coupling between these electronic states likely results in the observed disagreement between experiment and theory. A comparison between the electron affinities and term energies of aminomethoxy and other singly substituted alkoxy radicals $H_2C(R)O^\bullet$, ethoxy

(R=CH_3) and hydroxymethoxy (R=OH), provides physical insight into how the R group influences the electronic structure of these species. The observed trends in the EAs and T_0 of these radicals is associated with the strength of the intramolecular interaction between the R group and oxygen atom, with CH_3 being the weakest and OH strongest.

ASSOCIATED CONTENT

Supporting Information

The Supporting Information is available free of charge on the ACS Publications website at DOI:

Optimized geometries, rotational band shifts, additional spectra, vibrational assignments and a reproduction of the photoelectron spectrum of hydroxymethoxide.

AUTHOR INFORMATION

Corresponding Authors

*W. Carl Lineberger, e-mail: carl.lineberger@colorado.edu

*Julia H. Lehman, email: j.lehman@leeds.ac.uk

ORCID

W. Carl Lineberger 0000-0001-5896-6009

Julia H. Lehman 0000-0001-6610-6519

Present address

‡School of Chemistry, University of Leeds, Leeds LS2 9JT, United Kingdom

Notes

The authors declare no competing financial interest.

ACKNOWLEDGEMENTS

W.C.L. gratefully acknowledges significant contributions for this work from the NSF Physics Frontier Center Grant PHY1734006. J.H.L. also gratefully acknowledges support from Marie

Skłodowska Curie Actions – Individual Fellowship (MSCA-IF, Horizon 2020 grant 743642).

The authors thank Prof. Anne B. McCoy for insightful discussions on the vibrational activity of aminomethoxy. Dr. Joseph Beames and Dr. Yuri Aoto are gratefully acknowledged for their help with calculations in Molpro.

References

1. Atkinson, R., Atmospheric reactions of alkoxy and beta-hydroxyalkoxy radicals. *Int. J. Chem. Kin.* **1997,** *29*, 99-111.
2. Atkinson, R.; Carter, W. P. L., Reactions of Alkoxy Radicals under Atmospheric Conditions - the Relative Importance of Decomposition Versus Reaction with O_2. *J. Atmos. Chem.* **1991,** *13*, 195-210.
3. Davis, A. C.; Francisco, J. S., Hydroxyalkoxy Radicals: Importance of Intramolecular Hydrogen Bonding on Chain Branching Reactions in the Combustion and Atmospheric Decomposition of Hydrocarbons. *J. Phys. Chem. A* **2014,** *118*, 10982-1001.
4. Jungkamp, T. P. W.; Smith, J. N.; Seinfeld, J. H., Atmospheric Oxidation Mechanism of n-Butane: The Fate of Alkoxy Radicals. *J. Phys. Chem. A* **1997,** *101*, 4392-401.
5. Orlando, J. J.; Tyndall, G. S.; Wallington, T. J., The atmospheric chemistry of alkoxy radicals. *Chem. Rev.* **2003,** *103*, 4657-89.
6. Choo, K. Y.; Benson, S. W., Arrhenius Parameters for the Alkoxy Radical Decomposition Reactions. *Int. J. Chem. Kin.* **1981,** *13*, 833-44.
7. Davis, A. C.; Francisco, J. S., Reactivity Trends within Alkoxy Radical Reactions Responsible for Chain Branching. *J. Amer. Chem. Soc.* **2011,** *133*, 18208-19.
8. Fittschen, C.; Hippler, H.; Viskolcz, B., The beta C-C bond scission in alkoxy radicals: thermal unimolecular decomposition of t-butoxy radicals. *Phys. Chem. Chem. Phys.* **2000,** *2*, 1677-83.
9. Grana, R.; Frassoldati, A.; Faravelli, T.; Niemann, U*., et al.*, An experimental and kinetic modeling study of combustion of isomers of butanol. *Combust. Flame* **2010,** *157*, 2137-54.
10. Kochi, J. K., Chemistry of Alkoxy Radicals - Cleavage Reactions. *J. Amer. Chem. Soc.* **1962,** *84*, 1193-97.
11. Simmie, J. M.; Black, G.; Curran, H. J.; Hinde, J. P., Enthalpies of Formation and Bond Dissociation Energies of Lower Alkyl Hydroperoxides and Related Hydroperoxy and Alkoxy Radicals. *J. Phys. Chem. A* **2008,** *112*, 5010-16.
12. Vourliotakis, G.; Skevis, G.; Founti, M. A., Some aspects of combustion chemistry of C1-C2 oxygenated fuels in low pressure premixed flames. *Proc. Combust. Inst.* **2015,** *35*, 437-45.

13. Dupuis, M.; Wendoloski, J. J.; Lester, W. A., Electronic structure of vinoxy radical CH_2CHO. *J. Chem. Phys.* **1982,** *76*, 488-92.
14. Foster, S. C.; Hsu, Y. C.; Damo, C. P.; Liu, X.*, et al.*, Implications of the rotationally resolved spectra of the alkoxy radicals for their electronic structure. *J. Phys. Chem.* **1986,** *90*, 6766-69.
15. Gao, A.; Jiao, Z.; Li, A., The alkoxy radicals and their anions: Structures and electron affinities. *J. Mol. Struc.: Theochem* **2008,** *848*, 40-46.
16. Ramond, T. M.; Davico, G. E.; Schwartz, R. L.; Lineberger, W. C., Vibronic structure of alkoxy radicals via photoelectron spectroscopy. *J. Chem. Phys.* **2000,** *112*, 1158-69.
17. Shen, B. B.; Poad, B. L. J.; Continetti, R. E., Photoelectron−Photofragment Coincidence Studies of the tert-Butoxide Anion $(CH_3)_3CO^-$, the Carbanion Isomer $(CH_3)_2CH_2COH^-$, and Corresponding Radicals. *J. Phys. Chem. A* **2014,** *118*, 10223-32.
18. Tarczay, G.; Gopalakrishnan, S.; Miller, T. A., Theoretical prediction of spectroscopic constants of 1-alkoxy radicals. *J. Mol. Spectrosc.* **2003,** *220*, 276-90.
19. Yarkony, D. R., Nonadiabatic Quantum Chemistry - Past, Present, and Future. *Chem. Rev.* **2012,** *112*, 481-98.
20. Brossard, S. D.; Carrick, P. G.; Chappell, E. L.; Hulegaard, S. C.*, et al.*, The $^2A_1$–^2E electronic spectrum of methoxy, CH_3O: Vibrational progressions, and spin-orbit and Jahn–Teller couplings. *J. Chem. Phys.* **1986,** *84*, 2459-65.
21. Carter, C. C.; Atwell, J. R.; Gopalakrishnan, S.; Miller, T. A., Jet-cooled laser-induced fluorescence spectroscopy of some alkoxy radicals. *J. Phys. Chem. A* **2000,** *104*, 9165-70.
22. Ellison, G. B.; Engelking, P. C.; Lineberger, W. C., Photoelectron-Spectroscopy of Alkoxide and Enolate Negative-Ions. *J. Phys. Chem.* **1982,** *86*, 4873-78.
23. Endo, Y.; Saito, S.; Hirota, E., The microwave spectrum of the methoxy radical CH_3O. *J. Chem. Phys.* **1984,** *81*, 122-35.
24. Foster, S. C.; Misra, P.; Lin, T. Y. D.; Damo, C. P.*, et al.*, Free jet-cooled laser-induced fluorescence spectrum of methoxy. 1. Vibronic analysis of the A and X states. *J. Phys. Chem.* **1988,** *92*, 5914-21.
25. Gopalakrishnan, S.; Zu, L.; Miller, T. A., Radiative and non-radiative decay of selected vibronic levels of the B state of alkoxy radicals. *Chem.Phys.Lett.* **2003,** *380*, 749-57.
26. Inoue, G.; Akimoto, H.; Okuda, M., Laser-Induced Fluorescence-Spectra of CH_3O. *Chem.Phys.Lett.* **1979,** *63*, 213-16.
27. Inoue, G.; Okuda, M.; Akimoto, H., Laser-induced fluorescence of the C_2H_5O radical. *J. Chem. Phys.* **1981,** *75*, 2060-65.
28. Bent, G. D.; Adams, G. F.; Bartram, R. H.; Purvis, G. D.*, et al.*, Many-body perturbation theory electronic structure calculations for the methoxy radical. I. Determination of Jahn–Teller energy surfaces, spin–orbit splitting, and Zeeman effect. *J. Chem. Phys.* **1982,** *76*, 4144-56.
29. Domcke, W.; Yarkony, D. R., Role of Conical Intersections in Molecular Spectroscopy and Photoinduced Chemical Dynamics. *Annu. Rev. Phys. Chem.* **2012,** *63*, 325-52.
30. Höper, U.; Botschwina, P.; Köppel, H., Theoretical study of the Jahn–Teller effect in $\tilde{X}\ ^2ECH_3O$. *J. Chem. Phys.* **2000,** *112*, 4132-42.
31. Malbon, C. L.; Yarkony, D. R.; Zhu, X. L., On the electronic structure of the ground state of cyclopentoxy. The case for a two coupled state description. *J. Mol. Spectrosc.* **2015,** *311*, 36-41.
32. Barckholtz, T. A.; Miller, T. A., Quantitative insights about molecules exhibiting Jahn-Teller and related effects. *International Reviews in Physical Chemistry* **1998,** *17*, 435-524.

33. Jin, J.; Sioutis, I.; Tarczay, G.; Gopalakrishnan, S.*, et al.*, Dispersed fluorescence spectroscopy of primary and secondary alkoxy radicals. *J. Chem. Phys.* **2004,** *121*, 11780.
34. Liu, J. J.; Melnik, D.; Miller, T. A., Rotationally resolved $\tilde{B}$ δ $\tilde{X}$ electronic spectra of the isopropoxy radical: A comparative study. *J. Chem. Phys.* **2013,** *139*, 094308.
35. Liu, J. J.; Reilly, N. J.; Mason, A.; Miller, T. A., Laser-Induced Fluorescence Spectroscopy of Jet-Cooled t-Butoxy. *J. Phys. Chem. A* **2015,** *119*, 11804-12.
36. Alam, J.; Reza, M. A.; Mason, A.; Reilly, N. J.*, et al.*, Dispersed Fluorescence Spectroscopy of Jet-Cooled 2-, 3-, and 4-Methylcyclohexoxy Radicals. *J. Phys. Chem. A* **2015,** *119*, 6257-68.
37. Oliveira, A. M.; Lehman, J. H.; McCoy, A. B.; Lineberger, W. C., Photoelectron spectroscopy of the hydroxymethoxide anion, $H_2C(OH)O^-$. *J. Chem. Phys.* **2016,** *145*, 124317.
38. Danger, G.; Duvernay, F.; Theule, P.; Borget, F.*, et al.*, Hydroxyacetonitrile ($HOCH_2CN$) Formation in Astrophysical Conditions. Competition with the Aminomethanol, a Glycine Precursor. *Astrophys. J.* **2012,** *756*, 11.
39. Duvernay, F.; Danger, G.; Theule, P.; Chiavassa, T.*, et al.*, Formaldehyde Chemistry in Cometary Ices: On the Prospective Detection of NH_2CH_2OH, $HOCH_2OH$, and POM by the on-Board Rosina Instrument of the Rosetta Mission. *Astrophys. J.* **2014,** *791*, 75.
40. Feldmann, M. T.; Widicus, S. L.; Blake, G. A.; Kent Iv, D. R.*, et al.*, Aminomethanol water elimination: Theoretical examination. *J. Chem. Phys.* **2005,** *123*, 34304.
41. Hays, B. M.; Widicus-Weaver, S. L., Theoretical Examination of O(^{1}D) Insertion Reactions to Form Methanediol, Methoxymethanol, and Aminomethanol. *J. Phys. Chem. A* **2013,** *117*, 7142-48.
42. Blanksby, S. J.; Ellison, G. B., Bond dissociation energies of organic molecules. *Acc. Chem. Res.* **2003,** *36*, 255-63.
43. Sheps, L.; Miller, E. M.; Lineberger, W. C., Photoelectron spectroscopy of small $IBr^-(CO_2)_n$, (n=0-3) cluster anions. *J. Chem. Phys.* **2009,** *131*, 64304.
44. Lu, Y. J.; Lehman, J. H.; Lineberger, W. C., A versatile, pulsed anion source utilizing plasma-entrainment: Characterization and applications. *J. Chem. Phys.* **2015,** *142*, 44201.
45. Dick, B., Inverting ion images without Abel inversion: maximum entropy reconstruction of velocity maps. *Phys. Chem. Chem. Phys.* **2014,** *16*, 570-80.
46. Cooper, J.; Zare, R. N., Angular Distribution of Photoelectrons. *J. Chem. Phys.* **1968,** *48*, 942-43.
47. Sanov, A., Laboratory-Frame Photoelectron Angular Distributions in Anion Photodetachment: Insight into Electronic Structure and Intermolecular Interactions. *Annu. Rev. Phys. Chem.* **2014,** *65*, 341-63.
48. Neumark, D. M., Slow Electron Velocity-Map Imaging of Negative Ions: Applications to Spectroscopy and Dynamics. *J. Phys. Chem. A* **2008,** *112*, 13287-301.
49. Lineberger, W. C.; Woodward, B. W., High Resolution Photodetachment of S^- near Threshold. *Phys. Rev. Lett.* **1970,** *25*, 424-27.
50. Engelking, P. C., Approximate Rotational Band Shifts. *J. Phys. Chem.* **1986,** *90*, 4544-45.
51. Travers, M. J.; Cowles, D. C.; Clifford, E. P.; Ellison, G. B.*, et al.*, Photoelectron Spectroscopy of the CH_3N^- ion. *J. Chem. Phys.* **1999,** *111*, 5349-60.
52. Frisch, M. J.; Trucks, G. W.; Schlegel, H. B.; Scuseria, G. E.*, et al. Gaussian 09*, Gaussian, Inc.: Wallingford, CT, USA, 2009.

53. Werner, H. J.; Knowles, P. J.; Knizia, G.; Manby, F. R.*, et al.*, Molpro: a general-purpose quantum chemistry program package. *WIREs Comput. Mol .Sci.* **2012,** *2*, 242-53.
54. Dillon, J. J.; Yarkony, D. R., The photoelectron spectrum of the ethoxide anion: Conical intersections, the spin-orbit interaction, and sequence bands. *J. Chem. Phys.* **2009,** *131*, 134303.
55. Dillon, J.; Yarkony, D. R., Nonadiabatic effects in substitutional isomers of Jahn-Teller molecules: The strange case of hydroxymethoxy. *J. Chem. Phys.* **2012,** *137*, 154315.
56. Dillon, J. J.; Yarkony, D. R., The photoelectron spectrum of the isopropoxide anion: Nonadiabatic effects due to conical intersections and the spin-orbit interaction. *J. Chem. Phys.* **2009,** *130*, 154312.
57. Mozhayskiy, V. A.; Krylov, A. I. *ezSpectrum 3.0, available online at iopenshell.usc.edu/downloads*, 2016.
58. Sharp, T. E.; Rosenstock, H. M., Franck-Condon Factors for Polyatomic Molecules. *J. Chem. Phys.* **1964,** *41*, 3453-63.
59. Oliveira, A. M.; Lehman, J. H.; McCoy, A. B.; Lineberger, W. C., Photoelectron Spectroscopy of cis-Nitrous Acid Anion (cis-$HONO^-$). *J. Phys. Chem. A* **2016,** *120*, 1652-60.
60. Ervin, K. M.; DeTuro, V. F., Anchoring the gas-phase acidity scale. *J. Phys. Chem. A* **2002,** *106*, 9947-56.
61. Bohme, D. K.; Mackay, G. I.; Tanner, S. D., An experimental study of nucleophylic addition to formaldehyde in the gas phase. *J. Chem. Phys.* **1978,** *69*, 407-09.
62. Wickham-Jones, C. T.; Ervin, K. M.; Ellison, G. B.; Lineberger, W. C., NH_2 Electron-Affinity. *J. Chem. Phys.* **1989,** *91*, 2762-63.
63. Neumark, D. M.; Lykke, K. R.; Andersen, T.; Lineberger, W. C., Laser photodetachment measurement of the electron affinity of atomic oxygen. *Physical Review A* **1985,** *32*, 1890-92.
64. Weichman, M. L.; Cheng, L.; Kim, J. B.; Stanton, J. F.*, et al.*, Low-lying vibronic level structure of the ground state of the methoxy radical: Slow electron velocity-map imaging (SEVI) spectra and Köppel-Domcke-Cederbaum (KDC) vibronic Hamiltonian calculations. *J. Chem. Phys.* **2017,** *146*, 224309.
65. Adams, C. L.; Schneider, H.; Weber, J. M., Vibrational Autodetachment-Intramolecular Vibrational Relaxation Translated into Electronic Motion. *J. Phys. Chem. A* **2010,** *114*, 4017-30.
66. Lykke, K. R.; Mead, R. D.; Lineberger, W. C., Observation of Dipole-Bound States of Negative Ions. *Phys. Rev. Lett.* **1984,** *52*, 2221-24.
67. Lykke, K. R.; Neumark, D. M.; Andersen, T.; Trapa, V. J.*, et al.*, Autodetachment spectroscopy and dynamics of CH_2CN^- and CD_2CN^-. *J. Chem. Phys.* **1987,** *87*, 6842-53.
68. Marks, J.; Brauman, J. I.; Mead, R. D.; Lykke, K. R.*, et al.*, Spectroscopy and dynamics of the dipole-supported state of acetyl fluoride enolate anion. *J. Chem. Phys.* **1988,** *88*, 6785-92.
69. Mead, R. D.; Lykke, K. R.; Lineberger, W. C.; Marks, J.*, et al.*, Spectroscopy and dynamics of the dipole-bound state of acetaldehyde enolate. *J. Chem. Phys.* **1984,** *81*, 4883-92.
70. Nelson, D. J.; Gichuhi, W. K.; Miller, E. M.; Lehman, J. H.*, et al.*, Anion photoelectron spectroscopy of deprotonated ortho-, meta-, and para-methylphenol. *J. Chem. Phys.* **2017,** *146*, 074302.
71. Wang, L. S., Perspective: Electrospray photoelectron spectroscopy: From multiply-charged anions to ultracold anions. *J. Chem. Phys.* **2015,** *143*, 040901.
72. Weber, J. M.; Robertson, W. H.; Johnson, M. A., Argon predissociation and electron autodetachment spectroscopy of size-selected $CH_3NO_2^-$ Ar_n clusters. *J. Chem. Phys.* **2001,** *115*, 10718-23.

73. Weichman, M. L.; Kim, J. B.; Neumark, D. M., Rovibronic structure in slow photoelectron velocity-map imaging spectroscopy of CH_2CN^- and CD_2CN^-. *J. Chem. Phys.* **2014,** *140*, 104305.
74. Peterson, K. A.; Feller, D.; Dixon, D. A., Chemical accuracy in ab initio thermochemistry and spectroscopy: current strategies and future challenges. *Theo. Chem. Acc.* **2012,** *131*, 1079-5 (20 pp).
75. Jentschura, U. D.; Kotochigova, S.; LeBigot, E. O.; Mohr, P. J., *et al.* The Energy Levels of Hydrogen and Deuterium (version 2.1). Gaithersburg, MD, 2017.

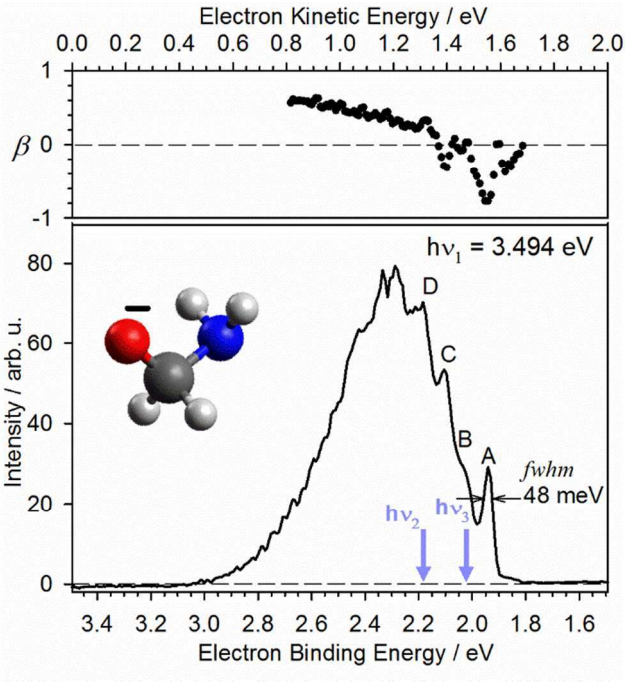

Figure 1: (Lower panel) Low resolution photoelectron spectrum of aminomethoxide obtained with a photon energy of 3.494 eV. Four apparent peaks are labelled A, B, C, and D. The arrows labelled $h\nu_2$ and $h\nu_3$ indicate photon energies used to obtain the higher resolution spectra shown in Figs. 2 and 3, respectively. (Upper panel) Photoelectron anisotropy parameter (β) of aminomethoxide (black dots) as a function of electron kinetic energy (eKE). The β values are only displayed where a significant photoelectron signal was observed.

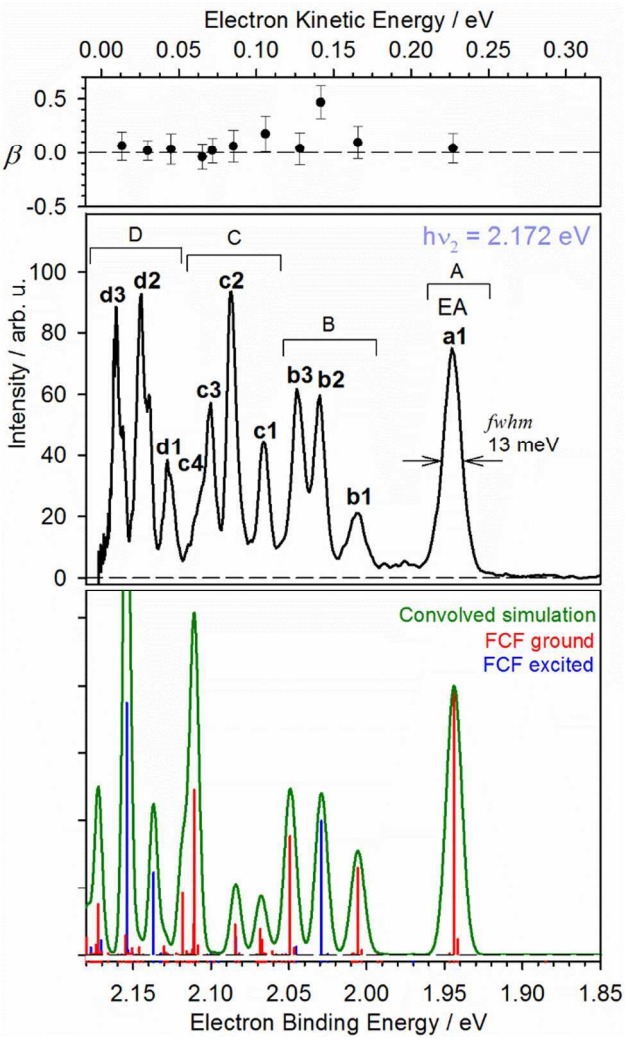

Figure 2: (Lower panel) Calculated photoelectron spectrum for transitions from the ground electronic state of aminomethoxide to the ground and first excited state of aminomethoxy radical. (Middle panel) Photoelectron spectrum obtained using a photon energy of 2.172 eV. The previously unresolved subpeaks in features A, B, C, and D of Fig.1 are now resolved and identified as a1, a2, etc. in this panel. (Upper panel) Anisotropy parameter β associated with the photoelectron spectrum found in the middle panel.

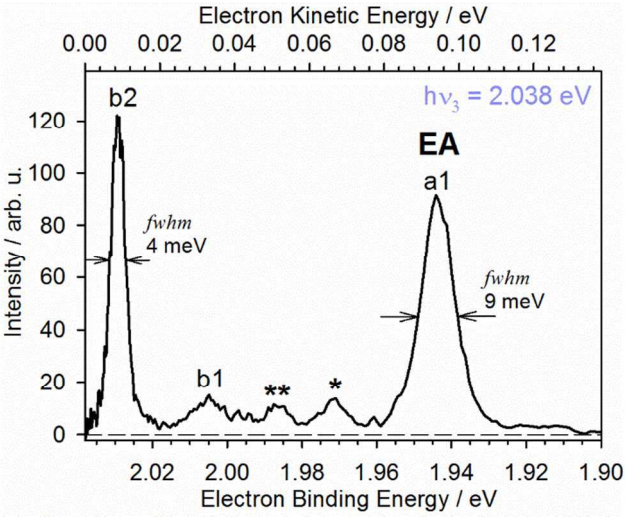

Figure 3: Aminomethoxide high resolution photoelectron spectrum obtained using a photon energy of $h\nu_3$=2.038 eV. The two peaks labelled * and ** are discussed further in the text.

Table 1: Summary of major results.

Summary of major results	**Experiment**	**Calculation**
EA($H_2C(NH_2)O^{\bullet}$) / eV	1.944(1)	1.89 eV[a]
$T_0(\tilde{A} \leftarrow \tilde{X})$ ($H_2C(NH_2)O^{\bullet}$) / eV	0.085(1)	0.201 eV[b]
$\Delta_{acid}H^{o}_{0K}(H_2C(NH_2)OH)$ / kcal mol^{-1}	-	374.0[c]
$D_0(H_2C(NH_2)O–H)$ / kcal mol^{-1}	106(2)[d]	107.7[c]
[a] CCSD(T)/aug-cc-pVTZ (RO method used for neutral)		
[b] CAS(5,4)//MRCI-F12/aug-cc-pVTZ, see Section II.b		
[c] G4 composite method, see Section IV.a		
[d] Value based on the thermochemical cycle (Eq. 1) using the calculated $\Delta_{acid}H^{o}_{0K}(H_2C(NH_2)OH)$ which has a predicted uncertainty of ~ 2 kcal mol^{-1} (see Ref. 77)		

Table 2: Comparison between electron affinities and term energies of small substituted alkoxy radicals, $H_2C(R)O$, R = H, CH_3, NH_2 and OH.

$H_2C(\mathbf{R})O$	EA / eV	$T_0(\tilde{A} \leftarrow \tilde{X})$ / cm^{-1}
H	1.5689(7)[a]	*62(1)*[b]
CH_3	1.712(4)[c]	364(1)[d]
NH_2	1.944(1)[e]	689(10)[e]
OH	2.220(2)[f]	~3300[f]
a. Weichman *et al.*[64] b. Spin orbit splitting, Brossard *et al.*[20] c. Ramond *et al.*[16] d. Jin *et al.*[33] e. this work f. Oliveira *et al.*[37]		

Table of contents graphic